Affine Versus Non-Affine Fibril Kinematics in Collagen Networks: Theoretical Studies of Network Behavior

Preethi L. Chandran

Victor H. Barocas[1]
e-mail: baroc001@umn.edu

Department of Biomedical Engineering,
University of Minnesota,
312 Church St. SE,
Minneapolis, MN 55455

The microstructure of tissues and tissue equivalents (TEs) plays a critical role in determining the mechanical properties thereof. One of the key challenges in constitutive modeling of TEs is incorporating the kinematics at both the macroscopic and the microscopic scale. Models of fibrous microstructure commonly assume fibrils to move homogeneously, that is affine with the macroscopic deformation. While intuitive for situations of fibril-matrix load transfer, the relevance of the affine assumption is less clear when primary load transfer is from fibril to fibril. The microstructure of TEs is a hydrated network of collagen fibrils, making its microstructural kinematics an open question. Numerical simulation of uniaxial extensile behavior in planar TE networks was performed with fibril kinematics dictated by the network model and by the affine model. The average fibril orientation evolved similarly with strain for both models. The individual fibril kinematics, however, were markedly different. There was no correlation between fibril strain and orientation in the network model, and fibril strains were contained by extensive reorientation. As a result, the macroscopic stress given by the network model was roughly threefold lower than the affine model. Also, the network model showed a toe region, where fibril reorientation precluded the development of significant fibril strain. We conclude that network fibril kinematics are not governed by affine principles, an important consideration in the understanding of tissue and TE mechanics, especially when load bearing is primarily by an interconnected fibril network. [DOI: 10.1115/1.2165699]

Introduction

The Extracellular Matrix (ECM) forms the framework for soft tissues, achieving a range of functionalities by varying arrangement of its two main structural constituents, collagen and proteoglycan. The former serves as a fibrous tensile element, and the latter as an isotropic, swelling-compression element. A tissue equivalent (TE) is an in vitro reconstituted gel of type I collagen fibrils, subjected to in vivo-like cellular compaction and remodeling [1,2]. As a hydrated interconnected network of one of the principle load-bearing ECM components, which cells recognize as physiological, the TE is an important lab-scale model of tissue behavior. The governing role of the microstructure in determining the overall TE mechanics is important for the understanding of the more complex tissue system and the engineering of artificial tissue scaffolds [3].

The TE microstructure is the result of an entropy-driven self-assembly [4,5] and cellular remodeling. Collagen monomers, in cold acidic solution, when neutralized and warmed to 37°C, undergo nucleation and form thin filaments [6,7]. Fibrils grow by lateral and axial associations among filaments [8–10] and the assembled monomers spontaneously cross-link, stabilizing the structure. Fibrils fuse laterally, and a highly interconnected water-retaining network or collagen gel results [11]. A TE is formed when contractile cells, such as fibroblasts, are included in the reconstitution mixture and entrapped in the network during gelation. Network interconnections transmit cellular traction forces, leading to the large-scale rearrangement and the compaction of the gel [12]. Noncovalent interfibril interactions cross-link the compacted structure, and a stiffer tissue-like TE forms.

The macroscopic mechanical behavior of TEs in uniaxial extension is well studied. The stress response, the following cycles of preconditioning, is J shaped [13–15]. An initial extensible, low-force region, commonly attributed to preconditioning-induced material creep, is followed by an exponential and then steeply linear region of force increase [16]. TEs have been found to be highly viscoelastic. In one study [17], uniaxial stress did not truly stabilize, even after extensive preconditioning, and showed hysteresis. The accompanying microstructural rearrangements, however, have been shown highly consistent. Tower et al. [13] observed TE birefringence to change and recover reproducibly with each cycle and without hysteresis. While this suggests that strain-induced fiber rearrangements are inherently elastic, the macroscopic stress viscoelasticity might be a friction-like dissipation accompanying the rearranging. Also, fiber reorientation was found to occur extensively during the creep phase of the stress response but not during the linear phase [13]. The J-shaped force curve seems to result from a fibril tendency to reorient rather than stretch, and from fibril reorientation being less costly than fibril stretch.

The specific tensile stress behavior has been found to depend on initial fiber orientation [13,18], fiber cross-link density [19,20], fibril density [8], fibril dimensions (length and diameter) [8], and the presence of other ECM constituents such as PGs [19]. The stiffness of acellular collagen gels increased with fibril density, but that of cell-contracted TEs decreased [16]. Any general accounting of the matrix mechanics, be it qualitative and quantitative, requires a microstructural perspective.

To our knowledge, little work has been done on modeling the microstructural kinematics of TEs, but a number of approaches have been used to model tissues with fibrous microstructure. Early approaches were phenomenological (extensively used to model tendon mechanics, describing the material as a combination of

[1]Corresponding author.

Contributed by the Bioengineering Division of ASME for publication in the JOURNAL OF BIOMECHANICAL ENGINEERING. Manuscript received January 23, 2004; final manuscript received October 21, 2005. Review conducted by Christopher Jacobs.

elastic and viscous elements or by data-fitted mathematical expressions [21]. Microstructure-based methods can be considered in three broad types, depending on the scale at which the fiber contribution is analyzed. In one approach, the fiber microstructure is incorporated into traditional continuum formulations, by introducing an additional phase-averaged stress field, anisotropic and acting along the local fiber direction, specified by the continuum strain field [22–24]. While the above method works with averaged microstructural information (volume fraction, fiber orientation, etc.), the composite method works at the discrete level of an individual fiber and the surrounding matrix [25–27]. The effective continuum properties of the composite unit cell are determined and applied to the larger material. At these scales, a fiber matrix interaction and load bearing can be treated in great detail. Another popular class of models operates between these two scales, at that of the fiber collection. The microstructure is approximated by statistical distributions describing a fiber state such as orientation or crimp; tissue response is considered the volume average of independent fiber and matrix response [28,29].

In TEs, the matrix material is mostly water and unable to contribute to load bearing, especially in extension. However, localized centers of contractile cells effect a global rearrangement of the fibril lattice [12,30], implying that fibrils are connected by cross-link-like interactions that transmit forces. Such interconnection-mediated load transfer is also suggested in the birefringence patterns of a collagen gel in confined compression [31]. Network-like load bearing is also suggested in certain fibrous tissue behavior. The mechanical response of skin specimens, with the ground substance differentially digested off, was found similar to that of the untreated ones [32]. In cartilage the swelling pressure of trapped proteoglycans is resisted by an interconnected fiber system [33,34]. Many models of flat fibrous tissues assume the strain energy stored primarily in a cross-linked fiber phase [28].

A common theme in the modeling of collective fiber systems is that each fiber is an independently acting unit, and its deformation continuous with the macroscopic continuum strain field. The latter assumption, popularly known as the affine model, has been particularly effective when the primary load transfer is between the fiber and the matrix. Since microscopic deformation is solely determined by the macroscopic field, it precludes higher levels of discrete analysis, that of fiber interaction and relative fiber arrangement. While the affine approach is simple and intuitive, it is not known whether it truly describes a networked fiber system. In his seminal paper on the structural modeling of flat fibrous tissues, Lanir [28] recognized their networked nature, but made a key assumption of affine behavior, arguing it to be "intuitively justified by multiplicity of interconnections." Recent studies, however, suggest that nonaffine behavior may be important. Billiar and Sacks [29] reported nonaffine fiber rearrangement in stretched samples of bovine pericardium. The deformation of the alveolar wall network of lung-tissue strips in uniaxial stretch was examined using flourescence imaging [35]. The microscopic strains were found inconsistent with that at the macroscopic level and were interpreted using a network model. Studies of random fiber networks used to simulate the actin microstructure in cytoskeleton, found the deformation in semiflexible cross-linked fibers to be dominated by bending and nonaffine [36,37].

In this study "micromeshes" generated to simulate the TE microstructure were subjected to homogenous uniaxial tensile strain. Two models were used to describe the underlying fibril kinematics—the network model where the fibers interacted among themselves and required to balance forces at interconnections, and the affine model where fibers deformed as independent units, the strain dictated solely at the macroscopic level and the response linearly additive. The macroscale and microscale responses resulting from use of both models were analyzed for systematic similarities and differences.

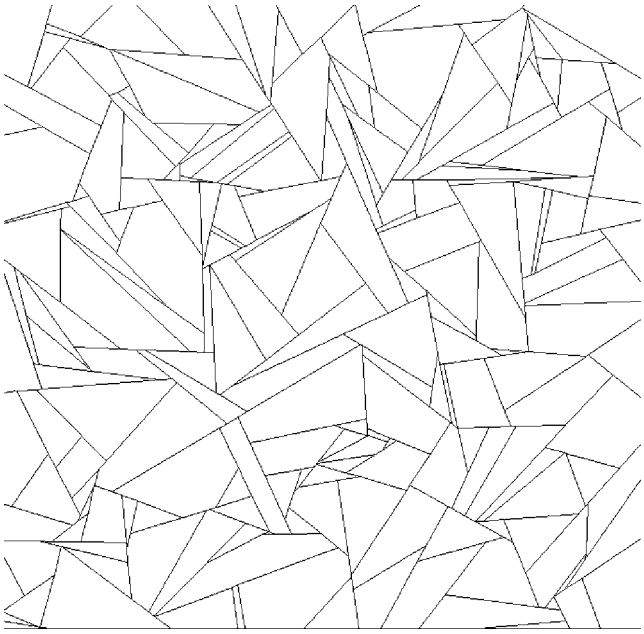

Fig. 1 Micromesh. A micromesh generated by growing segments from seed points and ending at intersections. Each intersection contains three segments, two of which are collinear. The mesh contains 553 segments.

Methods

Micromesh Generation. The following algorithm was used to construct the micromesh network and is based on the essential characteristics of the fibrillogenesis process discussed earlier.

(1) Random seed points were generated as nucleation sites for the growth of fibrils.
(2) Orientation of each growing fibril was assigned randomly.
(3) Each fibril grew at a uniform rate and continued growing until another fibril or an edge was hit. A cross-link formed at the contact, and the fibril stopped growing.

Once the network had been generated, the random seed points were no longer involved in the modeling. The cross-links are referred to as "nodes" and are modeled as pin joints (free rotation and no slipping through the joint), i.e., resistance to angle change was assumed negligible compared to fiber strain, consistent with a relatively small contact area for a cross-link and/or a high length/diameter ratio for the fiber segment. The nodes resemble chemical cross-links or physical cross-links that do not slip on the time scale of experiment. The line between two nodes, representing a portion of a collagen fibril, is referred to as a "segment." Micromeshes had nonoverlapping segments and three-segment junctions, where two of the three lay along a straight line (Fig. 1). Although the algorithm is readily extendable to three dimensions, only two dimensional networks are considered in the current work.

The micromeshes were compared, for their fiber angle and length distribution, to meshes reconstructed from TE confocal images. The Kolmogrov-Smirnov test was used to compare distribution data. Collagen gels were prepared as described previously [31], and compacted by Neonatal Human Dermal Fibroblasts (NHDFs) for one week to form TEs. Micrographs were obtained using a Biorad MRC 1000 confocal microscope, operating in the reflectance mode, with a 60X, 1.4 NA oil immersion lens (Nikon) and a quarter-wave plate. Fibril length and angle distribution data were obtained by tracing segments from 0.5 μm optical sections of the TE using ImageJ software. The traced area was considered

representative when the inclusion of surrounding fibers did not change the distributions significantly. The tracing was repeated on rotated images, and no significant change was observed in the distributions.

Segment Constitutive Equation. Collagen constitutive behavior is usually shown by a nonlinear stress–strain curve with a "toe" region of low elastic modulus, an upward rising "heel" region, and a highly stiff "linear" region. These curves are obtained from mechanical testing of collagen fiber systems (rat tail tendon, collagen gels) [16,38], where the behavior arises from a hierarchical arrangement of the collagen molecule. The toe region in the stress–strain curve of rat-tail tendon was found to coincide with the removal of fibril crimp, visible under a light microscope [38]. X-ray Synchrotron studies [39,40] implicated submicron-level rearrangement in the heel and toe region. The heel region corresponds to the straightening of kinks in the gap region of the fibril assembly. The reduction of disorder and therefore entropy causes a more rubber-like elasticity in this region [39]. In the linear region both intra-fibril (stretching of the triple helices and the crosslinks between the helices) as well as inter-fibril (inter-fibril slippage) events contribute [40]. It can thus be speculated that if the stress-strain curve were modified to retain only fibril material behavior, it would have no toe region and a steeper linear region.

In the model, however, additional factors were considered in specifying the fibril force-length curve. Fibrils were modeled as straight segments, and an artificial toe was introduced to model any slack in their initial state. Also, fibrils do not compress axially, but buckle. The resistance to buckling and accompanying steric hindrance was represented by a much lower stiffness in compression than in tension. The small level of intrafibril viscous effects reported occurring in the linear region [41] was neglected. Since it was not our intention to relate simulations to actual mechanical experiments, the fibril constitutive behavior was represented only in a qualitative sense. The segments were assumed to be of uniform diameter and behave elastically, the force being an exponential function of the Green's strain. The force function was similar to that used by Billiar and Sacks [42] in their microstructural modeling of fibrous tissues.

$$\mathbf{f}_s = A[\exp(BL_s) - 1] \tag{1}$$

where f_s is the force generated by a segment, A and B are material constants, and L_s is the segment Green's strain based on the segment stretch ratio λ_s.

$$L_s = 0.5(\lambda_s^2 - 1) \tag{2}$$

In the small strain limit, for a unit segment, Eqs. (1) and (2) reduce to a spring with spring constant $k=AB$. Figure 2 shows the segment force versus stretch ratio for $A=120$ nN and $B=2$ ($k=240$ nN), which was used for most of the simulations presented in this paper. In order to separate network effects from artifacts of the fibril segment equation, three other constitutive models were considered. First, Eq. (1) was used with $A=480$ nN, $B=0.5$, giving the same spring constant as $A=120$ nN, $B=2$, but a weaker nonlinear response. Second, a bilinear constitutive equation (cf. [25]) was considered, with different spring constants in tension and compression: $k=2$ nN in compression and 240 nN in tension. The third, a completely linear model with equal stiffness in compression and extension ($k=240$ nN). While the linear model is not representative of a fiber's inability to bear load in compression, it was included to identify fiber-induced versus network-induced nonlinearities. Although segment geometry and stiffness are to some degree arbitrary for this study, we note that an AB of 240 nN approximates to a Young's modulus of 60 MPa for a fibril diameter of 100 nm at a small strain region. Commonly reported moduli for collagen fibrils are on the order of 150–350 MPa [25,43].

Macroscopic Deformation: Homogeneous Uniaxial Strain. The sample was subjected to a prescribed stretch in one direction

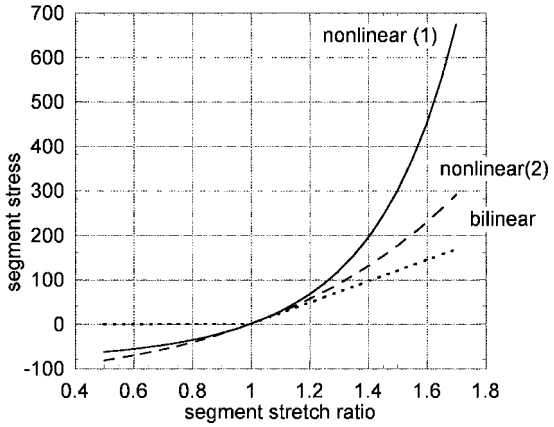

Fig. 2 Fibril constitutive equations. Four constitutive equations were used. The primary equation was Eq. (1) with $A=120$ nN and $B=2$, giving a highly nonlinear response in tension (solid line). The same equation was also used with $A=480$ nN and $B=0.5$ (dashed line), giving a weaker nonlinear response. A bilinear form with stiffness 240 nN in tension, and 2 nN in compression (dotted line), and a linear form with uniform stiffness 240 nN in extension and compression (not shown) were also considered. All four models gave a spring constant $k=240$ nN for small extensional strains of a unit fibril.

($\lambda_X > 1$), while maintained at zero stretch in the other direction ($\lambda_Y = 1$). In this configuration, no lateral compression in response to axial extension was allowed. While this deformation is reproduced experimentally only in strip biaxial testing with lateral grips held fixed [44,45], it allows solution of the microstructural kinematics problem with boundary displacements completely specified, eliminating the complexity of the Poisson effect on samples with free edges. Recognizing that most tests are performed in the simple uniaxial extension (with stress-free lateral edges), we chose the strip biaxial test as more conducive to relate the microscale and macroscale deformations.

Affine Model: Segment Kinematics and Macroscopic Behavior. Affine kinematics assumes each segment to deform independently, as though continuous with the macroscopic deformation. In two dimensions, the transformation is well established [46]. Given the macroscopic stretch ratios λ_X and λ_Y in the x and y directions, the stretch ratio (λ_s) and final orientation (θ_s) of a segment with initial orientation θ_{s0} is

$$\lambda_s^2 = \lambda_X^2 \cos^2 \theta_{s0} + \lambda_Y^2 \sin^2 \theta_{s0} \tag{3}$$

$$\theta_s = \tan^{-1}\left(\frac{\lambda_Y \tan \theta_{s0}}{\lambda_X}\right) \tag{4}$$

where angles are measured from the axis of stretch. For a given macroscopic stretch in the x direction, the degree of segment stretch is greater for segments aligned in the direction of the stretch (i.e., those for which the cosine term in (3) is large. Also, segments are recruited into the direction of stretch (since $\lambda_X/\lambda_Y < 1$, driving down θ_s (4))).

The macroscopic stress was obtained by averaging the total segment force over the area of the mesh. The segment force f_s was given by the constitutive equation (1), with λ_s determined solely by the initial segment orientation and the macroscopic stretch ratio. This model is similar to the Lanir-type structural models commonly used to describe fibrous tissue. The overall tissue response is considered the sum of microstructural responses, with the matrix contribution either negligible [42,47] or an isotropic hydrostatic pressure [28]. Our analysis uses a comparatively simplified fibril description, and a discrete fibril distribution versus a statistical one.

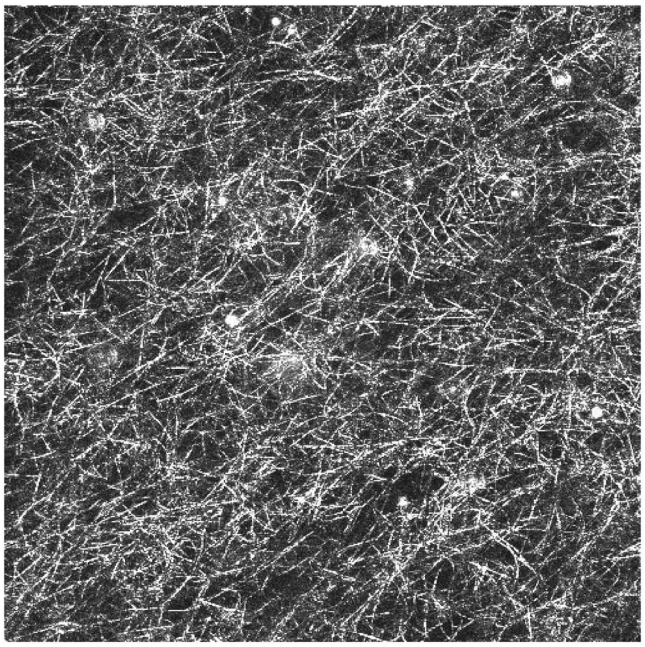

Fig. 3 Confocal micrograph of a tissue equivalent. The Image is a 110 μm square.

Network Model: Segment Kinematics and Macroscopic Stress–Strain Behavior. The macroscopic state of homogeneous uniaxial extension was applied by requiring boundary nodes to move affine with the macroscopic strain E. The internal nodal positions were required to be at equilibrium. The equations solved were

$$x_i = x_i(x_{i0}, E) \quad \text{on boundary nodes} \tag{5a}$$

$$\sum_s f_i^s = 0 \quad \text{on internal nodes} \tag{5b}$$

The subscript i indicates the two coordinate directions, x_{i0} is the initial coordinate of the node, and the summation (5b) is over segments intersecting at an internal node. The forces due to fiber bending or rotation through cross-links were considered negligible compared to the fiber stretch forces. The nonlinear problem (5) was solved using damped Newton-Raphson iteration.

The principles of Average Field theory were used to relate microscopic scale and macroscopic scale field variables [42,47]. In Average Field theory the macroscopic field variable is calculated as the volume average of a local microscopic field [48]. The approach is considered more physical, unlike the more mathematical Homogenization theory, which formulates the microstructure as fluctuations about an averaged behavior, obeying a periodic boundary condition [49–51]. Using Gauss' theorem, the volume average of a continuum variable can be expressed as the surface average of its discrete counterparts. Thus, the stress and strain tensors, T_{ij} and E_{ij}, describing macroscopic behavior in a volume V, can be related to the segment forces f^s and displacements u^s for all nodes on the surface S.

$$T_{ij} = 1/V \sum_s x_j^s f_i^s \tag{6a}$$

$$E_{ij} = 1/V \oint_S (n_i u_j + n_j u_i) dS \tag{6b}$$

where x^s is the nodal position vector and n^s is the unit normal vector to that surface. The derivation of Eqs. (6a) and (6b) is given in Appendix A. It is important to recognize that Eq. (6a) applies only to a system at microscopic equilibrium and could not be used for the affine model.

An average is a good description of discrete behavior only when the fields within the averaging volume are homogeneous in a statistical sense, i.e., the fluctuations due to a heterogeneous microstructure behave similarly everywhere within it. Under these conditions, the volume-averaged stress can be shown equivalent to the planar stress, defined as the average traction force across three mutually perpendicular planes (or two perpendicular lines in the 2-D case) within the material [52]. This was true in our case, for micromeshes containing at least 200 segments. We have also found [53,54] that for meshes of at least 200 segments, finite-domain artifacts in mesh generation and force calculation are negligible.

While Eq. (6b) provides an expression to calculate macroscopic strain from microscopic nodal displacements, it also implies that an average macroscopic strain can be imposed on the microscale by prescribing the displacement of the microscale boundary nodes. That is, when boundary nodes move affine with E_{ij}, the average strain of the network microstructure is also E_{ij}.

The network simulations were performed using the microstruc-

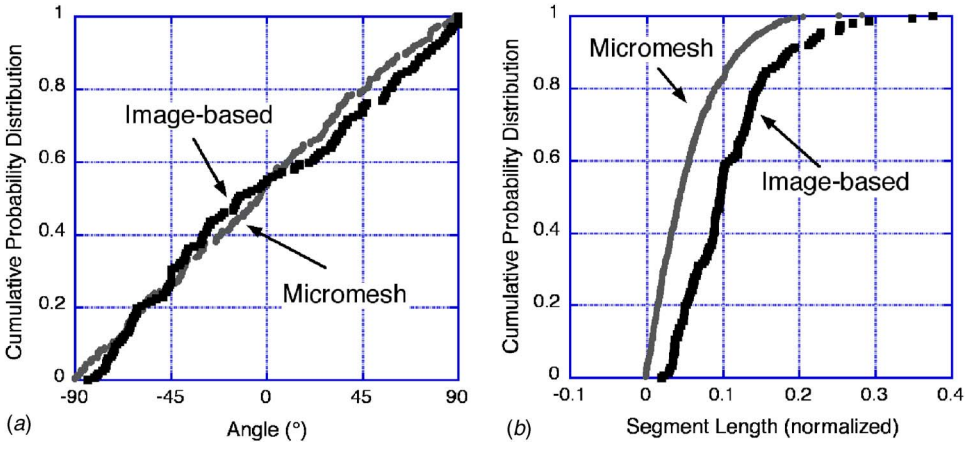

Fig. 4 Cumulative distribution functions TE and micromesh. Both the micromesh and the TE had a nearly uniform distribution of orientations (*a*). The segment length distributions (*b*) both possessed a wide uniform region, but the micromesh had many more very short segments and fewer very long segments.

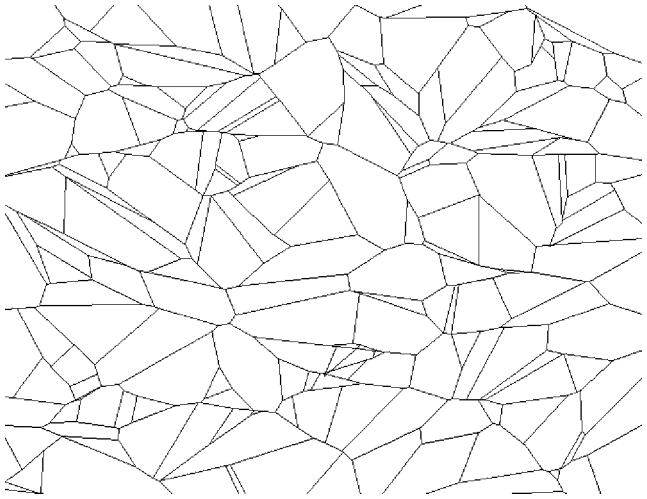

Fig. 5 Micromesh at 30% strain for the network model. The model shows significant rearrangement from the undeformed state (Fig. 1).

tural component of our algorithm developed to treat large networked materials in a multiscale manner [18]. Simulations were performed on an SGI Octane workstation.

Comparison of Models: Microscale Response. Scatter plots, with each data point relating an initial segment state to the final, were used to follow the discrete kinematics of a segment as a function of its initial state. Orientation, stretch ratio, and length of the segments were studied. Distributions were used to detect general trends within an entire microstructural state. A comparison of distributions was done with the Kolmogrov-Smirnov (K-S) test [55]. The K-S test determines the goodness of fit between two continuous distributions by computing a D statistic, defined as the maximum distance between the cumulative distribution functions (cdf) of the two samples. The null hypothesis that the two samples are drawn from the same parent distribution is rejected if

$$\sqrt{MN/(M+N)}D > D_{\text{crit}} \tag{7}$$

where M and N are the two sample sizes and D_{crit} is the critical D value for a given confidence level. The above expression applies for M and N greater than 80. Correlations between initial and final state variables were also used to quantify certain features of the microstructural response.

Comparison of Models: Macroscale Averaged Response. The averaged (macroscopic) response is not only the readily observable quantity on the laboratory scale, but is also the relevant one for describing material behavior as such. The two models were compared for their averaged response with respect to both the mechanical and geometric behavior of the microstructure.

While the stress σ_{XX} was chosen to indicate the net mechanical state, an orientation parameter Ω_{XX} was used to capture the net geometric state,

$$\Omega_{XX} = \frac{\sum_f l_s \cos^2 \theta_s}{\sum_s l_s} \tag{8}$$

If x is the direction of uniaxial stretch, the orientation parameter is defined as the xx component of the orientation tensor—i.e., the proportion of the total segment length cutting across the x plane in the x direction. For an isotropic network, $\Omega_{XX}=0.5$.

Results

Fiber Distribution in TE and Segment Distribution in Micromesh. Segment orientation and length distribution profiles were calculated from the confocal image of Fig. 3 and the 600-segment micromesh of Fig. 1. The TE orientation distribution was indistinguishable from a uniform distribution (Fig. 4(*a*), $p>0.1$), corresponding to an isotropic material. The length distributions were compared by scaling fiber/segment length by the total length (to match material density) in the image-based and the 600-segment micromesh (Fig. 4(*b*)). The cdfs were shifted relative to each other. There were no fibrils in the image-based mesh corresponding to the lower end of the segment length distribution for the micromesh.

Averaged Mechanical Behavior. The micromesh of Fig. 1 was subjected to uniaxial strain of up to 50%. The micromesh realization for the network model at 30% strain, shown in Fig. 5, is quite different in appearance from the initial network (Fig. 1). The macroscopic stress versus strain plots are shown in Fig. 6(*a*). Both the affine and network plots showed positive curvature with increasing strain. This could be expected given the nonlinear segment constitutive model and the progressive recruitment of segments in the direction of stretch. The network stresses were, however, much lower than the affine ones (e.g., about a factor of 3 lower at the 50% strain). Other micromesh realizations ($n=5$) of similar segment density and average orientation gave similar plots, to

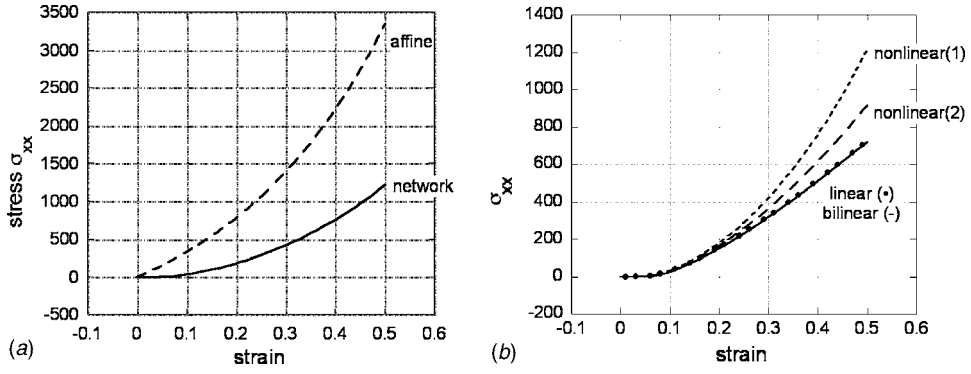

Fig. 6 Stress response in the micromeshes. (*a*) The affine model shows a much more rapid rise and a higher stress than the network model. (*b*) The network model gives similar stress response for each of the four constitutive equations described in Fig. 2. The toe region, the upward curvature, and the small stress compared to the affine model are present in all cases. The stresses in the linear (circles) and the bilinear (dotted) case were nearly indistinguishable.

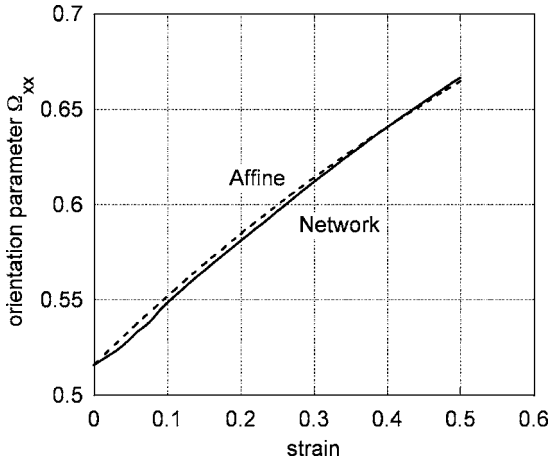

Fig. 7 Orientation response in the micromeshes. The network and affine models give similar values for the orientation parameter Ω_{XX} at all strains.

within 3% standard error, at any calculated strain.

A toe region of very low stress was seen at small strains in the network, but was absent in the affine case. The network toe region was also seen for bilinear and linear fibril stress–strain behaviors, where the fibril-level nonlinearities, fibril toe region, and low compressive stiffness, were systematically removed.

While there is no formal, quantitative definition of the toe region, a measure of the degree of toeing was made by defining ϵ_{toe} to be the strain at which the slope of the stress–strain curve was less than 1% of that for the linear region. For the curves of Fig. 6(*a*), the value of ϵ_{toe} was 7.4% for the network model and below 0.5% for the affine model. Figure 6(*b*) shows the stress–strain response for the same network model using the different segment constitutive equations of Fig. 2. Although there were small quantitative differences, the qualitative features, including the sharp upward curvature and the toe region, were preserved for all segment constitutive equations.

Averaged Geometric Behavior. The orientation parameter Ω_{XX} increased steadily in both the network and affine cases (Fig. 7). The overall trend in the network Ω_{XX} was not significantly different from the affine one.

Microscopic Observations—Segment Kinematics. The large-strain segment kinematic behavior (outside the toe region) is first examined, with the microstructural state at 30% strain taken as representative. Segment orientations at 30% strain are shown against the initial in Fig. 8(*a*). In the affine model, horizontal ($\cos^2\theta=1$) and vertical ($\cos^2\theta=0$) segments did not reorient, as there was no shear component of the macroscopic deformation acting on them. Segments in between oriented toward the stretch direction, in a manner described by (3). In the network case, however, the dependence of the final orientation on the initial was less evident (correlation coefficient=0.63 versus 0.99 for affine). Some vertical segments were recruited in the direction of stretch, and some horizontal segments reoriented away. Although the reorienting segments covered a wide range of angles toward and away from the stretch axis, independent of the initial orientation, there was an increased tendency to reorient toward the stretch axis ($\cos^2\theta=1$). This is seen by the rightward shift of the cdf in Fig. 8(*b*). The network and affine cdfs were significantly different ($p<0.001$).

The final segment stretch ratio is plotted against the initial orientation state in Fig. 9(*a*). The plot summarizes the influence of segment arrangement on material mechanics in the affine and network case. In an affine material, segments are increasingly stretched when more strongly oriented toward the stretch axis (3). Thus, vertical segments do not stretch whereas horizontal segments stretch as much as does the macroscopic boundary. In the network case, no such ready correlation between the final stretch state and initial orientation was seen. A wide range of stretch ratios occurred for any initial orientation state and tended toward moderate values, as can also be seen in the distribution profiles of Fig. 9(*b*) and 9(*c*). The affine model concentrated strain near the upper (right-hand) extreme of the distribution, forcing many fibers to experience nearly the full macroscopic strain. Segment compression ($\lambda_f<1$) was seen in the network, even though the overall domain is under homogenous stretch.

While no correlation between segment stretch ratio and orientation was evident for the network case ($p>0.1$ at 30% strain), a significant negative correlation ($r=-0.25, p<10^{-8}$) between the segment stretch ratio and the initial length was seen. In Fig. 10, the segment stretch ratio at 30% strain is plotted against the initial length for both the network and affine cases. In the network case, the larger stretch ratios were found always to occur in the smaller segments. Long segments were more likely to be in compression.

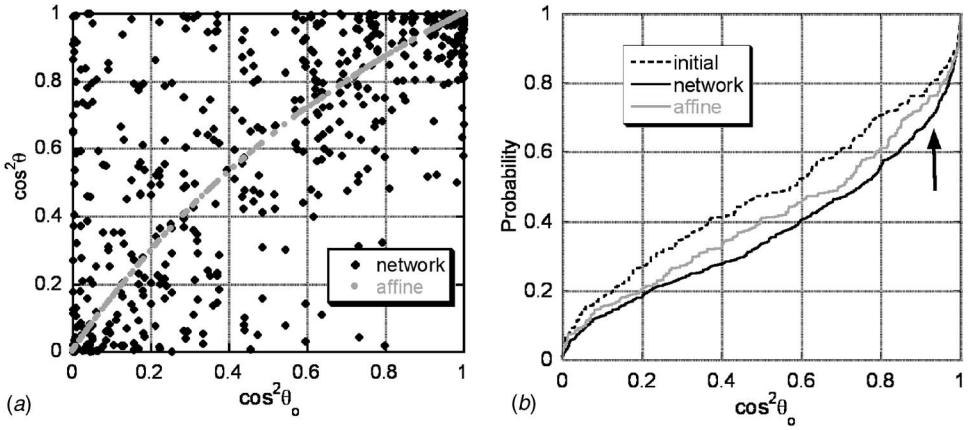

Fig. 8 Fibril kinematics—orientation. (*a*) Final orientation versus initial orientation for 30% strain. Each point represents a single segment. In the affine model, the final orientation is determined by initial orientation, so a smooth, monotonic curve results. In the network model, interactions among connected segments lead to much more scatter. (*b*) The cumulative distribution function is shifted farther to the right in the network model than in the affine model, indicating that more segments have been recruited into the direction of stretch.

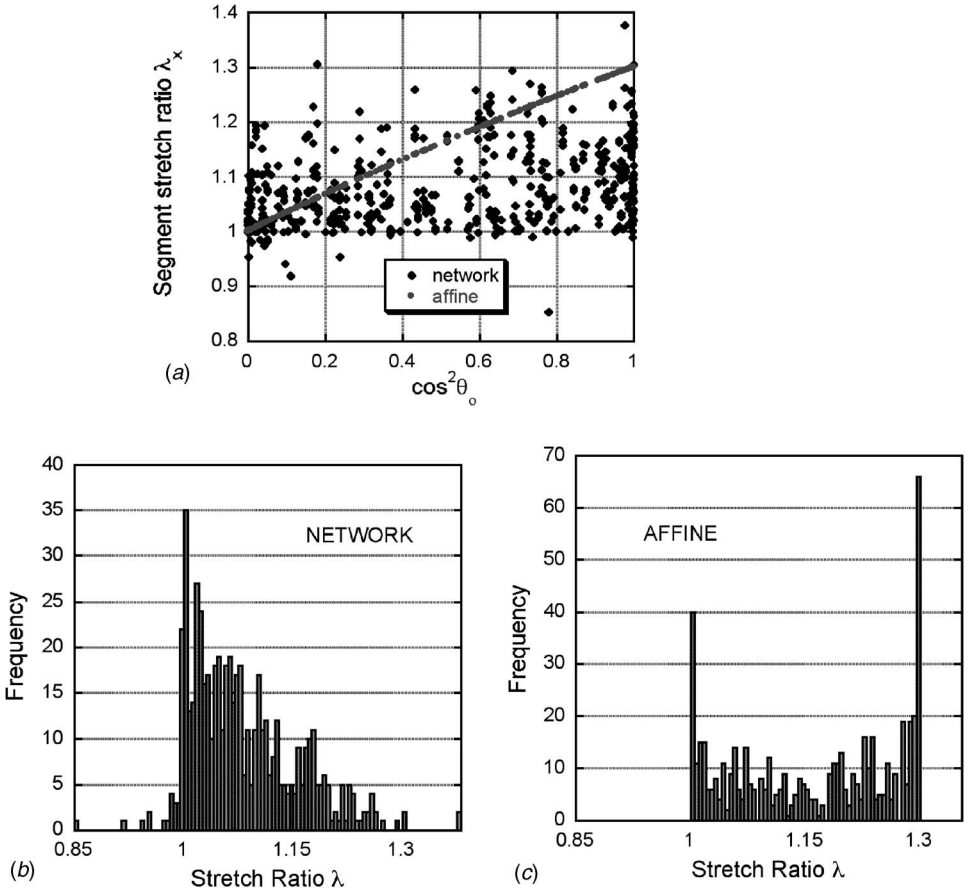

Fig. 9 Fibril kinematics—stretch. (*a*) Final segment stretch versus initial orientation for 30% strain. Because of the network's ability to rearrange, most segments experience less stretch in the network model than in the affine model. Some of the segments in the network model are in compression ($\lambda<1$). (*b*) The probability distribution function for the stretches shows much more stretch in the affine model.

The set of segments with length less than 0.05 contained 54% of the total segments, but 25% of the compressed fibers ($p<0.0003$).

The segment kinematics underlying the toe region of the stress–strain curve ($\epsilon<7.4\%$) were also examined by analyzing the network behavior at 4% strain. For the affine model, the segment stretch distribution at 4% strain was, as expected, similar to that at 30% strain, but less pronounced. Segments aligned with the stretch direction were stretched 4%, and those perpendicular to the stretch direction were neither stretched nor rotated. In the network model, however, very different behavior occurred, with almost all the macroscopic strain being taken up by reorientation rather than stretch. Of the 553 segments in the mesh, only 18 experienced strains greater than 0.1%, of which only 9 were greater than 2%.

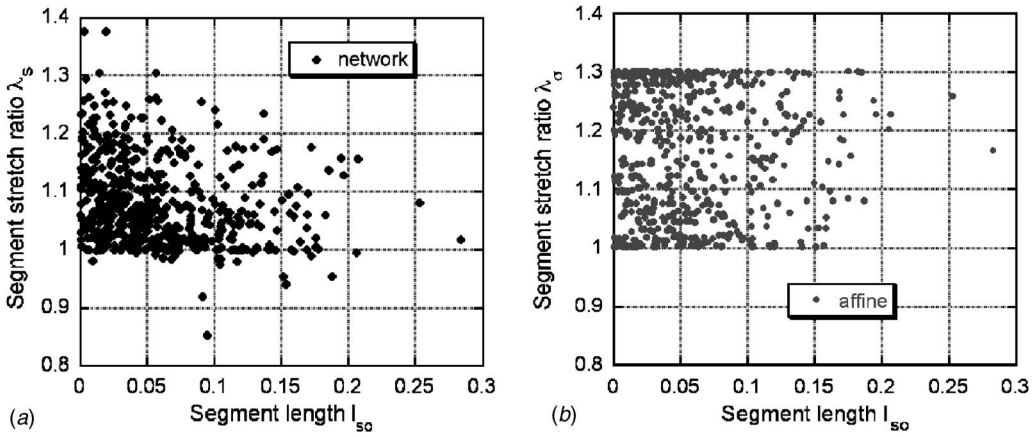

Fig. 10 Fibril Kinematics—stretch versus initial length. The network model (*a*) shows a negative correlation between initial length and stretch, but the affine model (*b*) does not.

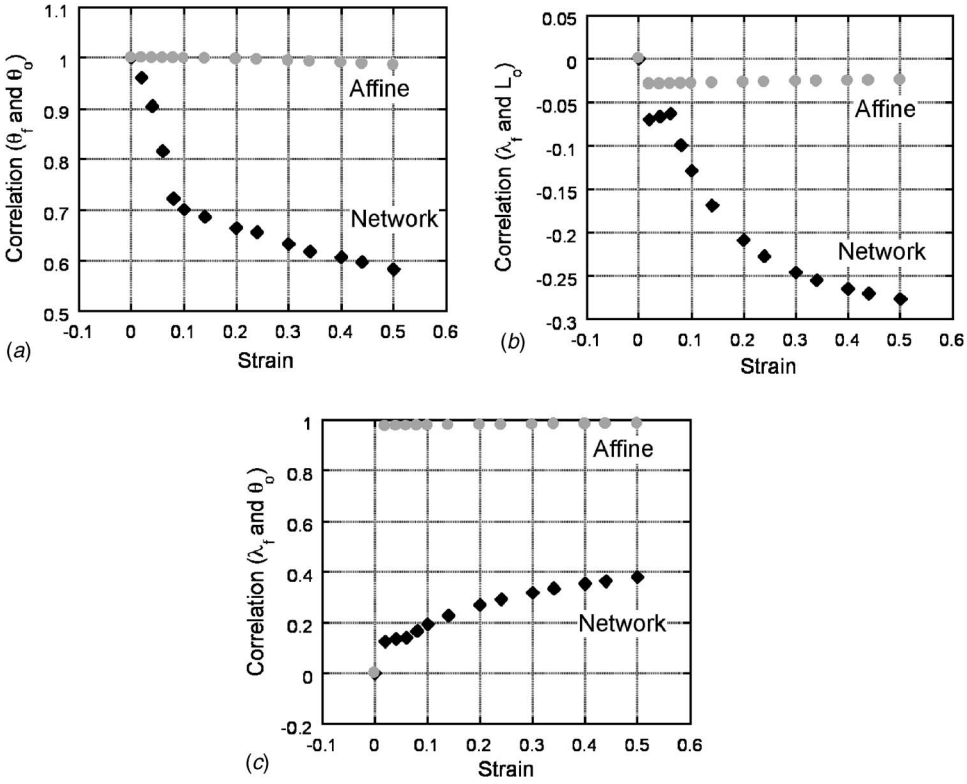

Fig. 11 Fibril kinematics—correlations. The differences between affine and network behavior, reflected in the scatter plots of Figs. 8–10, are quantified as correlation coefficients and plotted against strain. Correlations are shown for (*a*) initial angle θ_0 and final angle θ_f; (*b*) initial length L_0 and final stretch ratio λ_f; and (*c*) initial angle and final stretch ratio. Especially in the first two correlations, the network showed a shift in behavior at the end of the toe region.

In the affine model, roughly half the segments experienced strains greater than 2%. As in the large-strain region, the larger (i.e., the nonzero) segment strains occurred in the shorter segments for all micromesh realizations.

Functional Dependencies in Segment Kinematic Behavior—Correlation of Final Segment State to Initial. The scatter plots show different dependencies operating in the affine and network model, between a segment's initial and final state (orientation, length, and strain). The nature and magnitude of these dependencies vary with strain, markedly between the small and large strain region of the network. The relation between the initial and final state shown in scatter plots, can be summarized and tracked as changes in correlation coefficient behavior (Fig. 11).

In the affine case, the initial and final segment orientations remained closely correlated throughout (Fig. 11(*a*)). In the network case, the two quantities decorrelated increasingly with strain. The decorrelation was especially rapid within the toe region. Outside the toe region, the decorrelation was slower, and the pace was closer to that seen in the affine case. Figure 11(*b*) shows the correlation between the initial segment length and the final stretch ratio. While the two quantities remained completely uncorrelated in the affine case, an inverse correlation developed and increased steadily in the large-strain region of the network case. The inverse correlation did not increase within the toe region, since most segments were still unstrained. Figure 11(*c*) shows the correlation between the initial segment orientation and the final stretch ratio. In the affine case, the two remained highly correlated throughout (5). In the network case, the correlation was poor, especially in the toe region. The correlation increased slowly in the large strain region.

Large-Strain Behavior. From the correlation plots of Fig. 11, it is apparent that the network model underwent a different rearrangement strategy compared to the affine model. The differences were large and developed rapidly in the toe region. Outside the toe, in the large strain region, the network and affine correlation trends seemed more comparable. For example, network stretch ratios began to correlate slightly with initial orientation (Fig. 11(*c*)), and the final and initial orientations did not decorrelate as rapidly. The following question arises—once the extensive rearrangement capacity of the network is exhausted within the toe region, do network kinematics become increasingly affine? To explore this question, a "mixed" model was used, in which the micromesh of Fig. 1 was first prestretched past the end of the toe region (10% strain) in the network mode but then switched to the affine mode for larger strains. The stress in the mixed model at 50% strain was 2000, compared to 1300 for the pure network model and 3200 for the pure affine model, indicating that nonaffine effects are important, even at large strain (more detail in Ref. [54]).

Discussion

In reconstructing the mesh from confocal images of a TE, effort was made to remain true to the actual arrangement as well as its two-dimensional projection. Possible reconstruction errors include the detection of fibril slideover points as cross-links and vice versa, nonrandomness of the sampling, two dimensionalization of the 3-D sample, and any artifacts introduced by the imaging process. It is also possible that the compaction by fibroblasts changes the structure of the collagen network. While these errors must be considered in any conclusion, the fibril orientation distribution of the image-reconstructed mesh resembled a uniform distribution.

Correspondingly, micromeshes with segment directions assigned randomly consistently gave a uniform orientation cdf at the 600-segment level used. The length cdfs of the image-reconstructed and micromesh were shifted relative to each other. This could be a real difference or an artifact created by poor detectability of small-length fibrils, errors in fibril length scaling, or the other reconstruction errors. The micromesh did, however, match two important qualitative features of the image-based cdf. Both exhibited a large roughly linear region (corresponding to a uniform distribution of segment lengths) and a "tail" of relatively low-probability longer segments. We therefore conclude that the micromesh is a reasonable if not perfect representation of the fibril distribution in a collagen network. The simulation did not include a distribution of fibril diameters and being two-dimensional was limited in its representation of network topology. However, the simulation results described were observed in other test topologies [44] and only required a distribution of heterogeneities in the microstructure to show the difference between affine and network behavior. Also, given our intention to understand qualitatively the microscale and macro-scale mechanics in a TE, we expect the unaccounted fibril dynamics (fibril sliding, viscoelasticity, three dimensional arrangement space, relative bending to stretching stiffness) to be a bigger limitation than reproduction of the TE network architecture.

On the averaged (macroscopic) scale, the network model displayed much lower stresses than the affine model, but the averaged anisotropy in segment arrangement, reflected by the orientation parameter Ω_{XX}, evolved in a comparable manner for both models. The averaged orientation behavior did not reveal an important difference in the microscale orientation behavior. While the affine segment reorientations were correlated with the initial orientations, the network reorientations were not and tended more toward the macroscopic stretch axis.

In the affine case, the final segment orientation and stretch ratio were completely defined by the macroscopic deformation and the initial orientation state. In the network model, however, no such dependencies were observed. Instead, the segment stretch ratios were found to correlate inversely with segment length. Most segment stretch ratios were distributed within moderate levels, unlike the affine case where stretch ratios accumulated at the higher end. Thus the network minimizes the total stress within it, not only by redistributing segment strain to occur predominantly at moderate levels, but also by limiting the number of strained units (by confining the large strain to the smaller segments).

The network model showed a toe region for strains below 10%, within which the macroscopic stresses remained small. The toe region reflects a region where the network is able to accommodate the macroscopic strain by segment reorientation with minimal segment stretching. The segments recruited to stretch were again the lower length ones. The presence of the toe region was conserved for all segments of constitutive behavior used.

A distinct change in segment kinematics accompanied the transition from the toe to the large-strain region. At large strain, the stresses increased as segments concurrently stretched and reoriented. The reorientations, however, were less extensive (Fig. 11(*a*)) and a correlation between the stretch ratio and initial orientation seemed to develop, as in the affine model. Unlike the affine model, the network continued using the smaller segments to store strain (the corresponding negative correlation therefore increasing, Fig. 11(*b*), and containing the segment strains in the moderate range). A prestretched micromesh therefore gave much lower stresses when stretched into the large strain region in the network mode than in the affine mode, even though the segment reorientations were comparable. Moderate strains, inversely correlated with the segment length, are intrinsic to the network solution, irrespective of the reorientation capacity or even the microstructural arrangement. Also, depending on a certain tightness in the segment arrangement, the network can be in the toe region, where reorientation is free and extensive, or in the large-strain region, where reorientation is constrained and resembles the affine solution.

Nonaffine kinematics have been observed in experiments, [29,35] but the nature of the discrepancies are not clear. This study dealt only with the kinematics of one deformation (uniaxial stretch) and cannot account for macroscopic heterogeneity of the deformation field. Furthermore, the unit square model has no natural mechanism to incorporate stress boundary conditions, which occur frequently both in vivo and in vitro. A multiscale approach [18,51,53] would be needed to handle the greater complexity of a realistic loading scenario.

One would like to describe the overall behavior of a microstructured material in terms of average measures. These averages, or fabrics, quantify the microstructural arrangement [48] and are amenable to experimental determination. The orientation parameter Ω_{XX} is the simplest and most common fabric [48]. The stress parameter φ_{XX} is similar to Ω_{XX}, except that is it normalized by the total cell volume (i.e., the area in our 2-D calculations) rather than the total segment length [56]:

$$\varphi_{xx} \equiv \frac{\sum_s l_s \cos^2 \theta_s}{A} \tag{9}$$

where A is the area of the sample. The stress parameter is the number of segment units per volume that would cut across an x-facing plane in the x direction, thus contributing to the xx component of the stress; it is proportional to the number of collagen monomers aligned in the x direction per unit volume, corresponding to the quantity that would be measured by birefringence (birefringence would measure a quantity related to $\varphi_{XX}-\varphi_{YY}$ [57]).

Figures 7 and 12 show little difference in Ω_{XX} and φ_{XX} between the network and the affine models. The similarity in φ_{XX} and large difference in stress suggest that birefringence-based methods, although rapid and nondestructive, may not capture all important features of the microstructural response. This question requires further consideration, however, because numerous issues are not addressed by the simple analysis here—e.g., fibril stretch versus uncrimping, volume conservation, and intrafibril alignment of the monomer. Confocal microscopy [8] and small-angle light scattering [29] can provide more information on the overall orientation state of the network but are much less attractive because of time, localization, and sample handling issues.

The failure of φ_{XX} to reflect the large difference in stress between the network and affine models arises because φ_{XX} captures the number of fiber segments contributing to the stress but not the amount of the contribution. In the affine model, the segment stretch is highly correlated with orientation (cf. Fig. 11(*c*)), so a distinction between the number of contributing units and the amount of contribution is unnecessary. In the network case, however, reorientation can occur without stretch, so φ_{XX} predicts macroscopic stress poorly. To account for uncorrelated stretch and reorientation, a new parameter ψ_{XX} is proposed. A segment of length l_s contributes l_s units of segment stretch λ_s, projected in the xx direction by a factor of $\cos^2 \theta$. Therefore the total stretch per unit volume is given as

$$\psi_{XX} \equiv \frac{\sum_f \lambda_s l_s \cos^2 \theta_s}{A} \tag{10}$$

and should be a good predictor of the stress response. The quantity ψ_{XX} is plotted against strain in Fig. 12(*b*). The qualitative

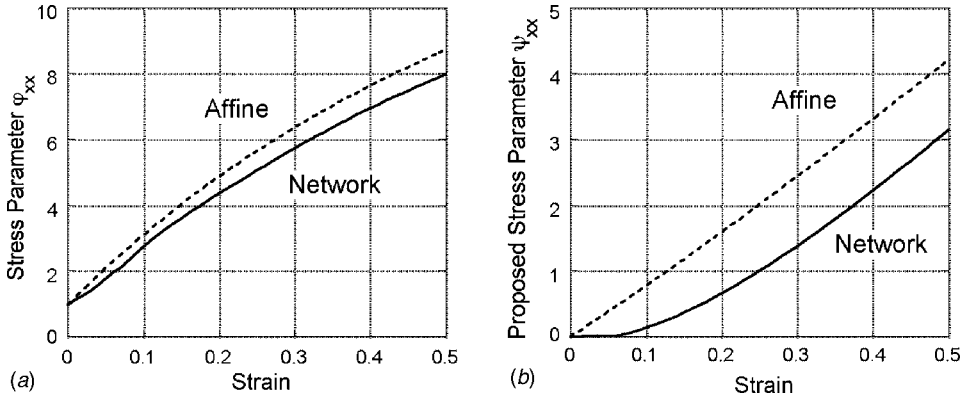

Fig. 12 Stress parameters. The standard stress parameter φ does not capture the differences between affine and network reorientation (*a*), but the modified stress parameter ψ of Eq. (12), as does (*b*).

features—toe region and much greater response in the affine than in the network model—are present as in the stress–strain curve.

In conclusion, for the deformation field studied in this paper, uniaxial stretch without lateral strain, the microstructural kinematics differed significantly between the network and affine models, with smaller stresses arising in the network case. Network behavior was characterized by extensive segment reorientation, moderate stretch ratios, and a concentration of the largest strains in the shortest segments. By requiring forces to balance at each node, the network model acts more like a uniform-stress model (or, equivalently, a strain–energy-minimization model). Also, because of the reorientation capacity of the network, it can take advantage of "looseness" in the segment arrangement to keep stresses low, leading to a toe region in the macroscopic stress–strain curve. These observations raise two questions. The first relates to the observation that the larger strains are concentrated in the shorter segments. The network problem may be thought of as a constrained minimization, in which the total strain energy is minimized subject to the requirements of macroscopic deformation and network connectivity. Why the solution to this problem involves larger strains in shorter segments is not immediately clear. The second question is how can one quantify the "looseness" of a network and thus anticipate how large a toe region will be effected by network rearrangement? Again, the answer will require further study.

The critical factor in deciding whether network effects could be significant for a given tissue or TE is the relationship between the fibril network and the surrounding material, which may include other structural proteins, proteoglycans, and/or cells. If the major mechanism for force transmission to a fibril is via other fibrils, then affine kinematics are unlikely and network dynamics should be considered; if the major mechanism is via the surrounding material, then the fibrils will tend to behave independently of each other and approach affine kinematics. TEs are obviously an extreme case of the former, having essentially no non-network solid component. The dense layer of the fetal membrane amnion [58,59] would be another example of a material for which network effects could be important, given its highly collagenous (with trace elastin) and relatively acellular nature. In contrast, the medial layer of the artery contains a high density of elastin and smooth-muscle cells, suggesting that affine fiber kinematics could be more likely for the fibrils (although other effects from the microscale inhomogeneity of the tissue would be important). Small angle light scattering experiments on bovine pericardium and porcine aortic valve [29] showed markedly nonaffine behavior at large strains, suggesting a nonaffine approach would be needed to capture the microstructural kinematics of those tissues, either due to network or other microstructural effects.

Acknowledgment

This work was supported primarily by the MRSEC Program of the National Science Foundation under Award Number DMR-9809364. Calculations were done using a resources grant from the University of Minnesota Supercomputing Institute. The assistance of Michael Rother and Afton Ellis is gratefully acknowledged.

Appendix

If T_{ij} and E_{ij} are macroscopic representations of the microscopic stress and strain field σ_{ij} and ϵ_{ij} within volume V of the material, the Average Field Theory [60] describes them to be

$$T_{ij} = \frac{1}{V}\int_V \sigma_{ij}\, dV \equiv \langle \sigma_{ij} \rangle \tag{A1}$$

$$E_{ij} = \frac{1}{V}\int_V \epsilon_{ij}\, dV \equiv \langle \epsilon_{ij} \rangle \tag{A2}$$

Equation (A1) can be rewritten as follows, noting that we employ the index notation summation convention

$$T_{ij} = \frac{1}{V}\int_V \sigma_{ik}\delta_{jk}\, dV \tag{A3}$$

$$T_{ij} = \frac{1}{V}\int_V \sigma_{ik}x_{j,k}\, dV \tag{A4}$$

$$T_{ij} = \frac{1}{V}\int_V (x_j\sigma_{ik})_{,k}\, dV - \frac{1}{V}\int_V X_j\sigma_{ik,k}\, dV \tag{A5}$$

Applying the divergence theorem to the first term,

$$T_{ij} = \frac{1}{V}\oint_s n_k x_j \sigma_{ik}\, dS - \frac{1}{V}\int_V x_j\sigma_{ik,k}\, dV \tag{A6}$$

The second term vanishes by the requirement of local equilibrium, $\sigma_{ik,k}=0$.

$$T_{ij} = \frac{1}{V}\oint_s n_k x_j \sigma_{ik}\, dS \tag{A7}$$

The continuous traction $n_k\sigma_{ik}$ at the boundary is supplied by the discrete fiber forces f_i at the boundary nodes,

$$T_{ij} = \frac{1}{V}\oint_s n_k x_j \sigma_{ik}\, dS = \oint_s x_j f_i\, dS = \frac{1}{V}\sum_s x_j f_i \tag{A8}$$

The above averaged stress tensor T_{ij} is symmetric [61].

Similarly the average strain in Eq. (A2) can be shown completely determined by the displacement of the boundary nodes.

$$E_{ij} = \frac{1}{V}\int \varepsilon_{ij}\, dV = \frac{1}{V}\int (u_{i,j} + u_{j,i})\, dV = \oint_s (n_i u_j + n_j u_i) dS \tag{A9}$$

The above formulation is rotationally invariant [61].

References

[1] Bell, E., Ivarsson, B., and Merrill, C., 1979, "Production of a Tissue-Like Structure by Contraction of Collagen Lattices by Human Fibroblasts of Different Proliferative Potential in vivo," Proc. Natl. Acad. Sci. U.S.A., **76**, pp. 1274–1278.

[2] Tranquillo, R. T., 1999, "Self-Organization of Tissue-Equivalents: The Nature and Role of Contact Guidance," Biochem. Soc. Symp., **65**, pp. 27–42.

[3] Tranquillo, R. T., Durrani, M. A., and Moon, A. G., 1992, "Tissue Engineering Science–Consequences of Cell Traction Force," Cytotechnology, **10**, pp. 225–250.

[4] Veis, A., 1982, "Collagen Fibrillogenesis," Connect. Tissue Res., **10**, pp. 11–24.

[5] Kadler, K. E., Holmes, D. F., Trotter, J. A., and Chapman, J. A., 1996, "Collagen Fibril Formation," Biophys. J., **316**, pp. 1–11.

[6] Piez, K. A., 1982, "Structure and Assembly of the Native Collagen Fibril," Connect. Tissue Res., **10**, pp. 25–36.

[7] Suarez, G., Oronsky, A. L., Bordas, J., and Koch, M. H., 1985, "Synchrotron Radiation X-Ray Scattering in the Early Stages of *In Vitro* Collagen Fibril Formation," Proc. Natl. Acad. Sci. U.S.A., **82**, pp. 4693–4696.

[8] Roeder, B. A., Kokini, K., Surgis, J. E., Robinson, J. P., and Voytik-Harbin, S. L., 2002, "Tensile Mechanical Properties of Three-Dimensional Type I Collagen Extracellular Matrices With Varied Microstructure," J. Biomech. Eng., **124**, pp. 214–223.

[9] Holmes, D. F., Graham, H. K., Trotter, J. A., and Kadler, K. E., 2001, "STEM/TEM Studies of Collagen Fibril Assembly," Micron, **32**, pp. 273–285.

[10] Brightman, A. O., Rajwa, B. P., Sturgis, J. E., McCallister, M. E., Robinson, J. P., and Voytik-Harbin, S. L., 2000, "Time-Lapse Confocal Reflection Microscopy of Collagen Fibrillogenesis and Extracellular Matrix Assembly *In Vitro*," Biopolymers, **54**, pp. 222–234.

[11] Zhu, W., Iatridis, J. C., Hlibczuk, V., Ratcliffe, A., and Mow, V. C., 1996, "Determination of Collagen–Proteoglycan Interactions *In Vitro*," J. Biomech., **29**, pp. 773–783.

[12] Grinnell, F., and Lamke, C. R., 1984, "Reorganization of Hydrated Collagen Lattices by Human Skin Fibroblasts," J. Cell. Sci., **66**, pp. 51–63.

[13] Tower, T. T., Neidert, M. R., and Tranquillo, R. T., 2002, "Fiber Alignment Imaging During Mechanical Testing of Soft Tissues," Ann. Biomed. Eng., **30**, pp. 1221–1233.

[14] Feng, Z., Yamato, M., Akutsu, T., Nakamura, T., Okano, T., and Umezu, M., 2003, "Investigation on the Mechanical Properties of Contracted Collagen Gels as a Scaffold for Tissue Engineering," Artif. Organs, **27**, pp. 84–91.

[15] Ozerdem, B., and Tozeren, A., 1995, "Physical Response of Collagen Gels to Tensile Strain," ASME J. Biomech. Eng., **117**, pp. 397–401.

[16] Chapuis, J. F., and Agache, P., 1992, "A New Technique to Study the Mechanical Properties of Collagen Lattices," J. Biomech., **25**, pp. 115–120.

[17] Wagenseil, J. E., 2003, "One-Dimensional Viscoelastic Behavior of Fibroblast Populated Collagen Matrices," J. Biomech. Eng., **125**, pp. 719–725.

[18] Agoram, B., and Barocas, V. H., 2001, "Coupled Macroscopic and Microscopic Scale Modeling of Fibrillar Tissues and Tissue Equivalents," J. Biomech. Eng., **123**, pp. 362–369.

[19] Sheu, M. T., Huang, J. C., Yeh, G. C., and Ho, H. O., 2001, "Characterization of Collagen Gel Solutions and Collagen Matrices for Cell Culture," Biomaterials, **22**, pp. 1713–1719.

[20] Osborne, C. S., Barbenel, J. C., Smith, D., Savakis, M., and Grant, M. H., 1998, "Investigation Into the Tensile Properties of Collagen/Chondroitin-6-Sulphate Gels: The Effect of Crosslinking Agents and Diamines," Med. Biol. Eng. Comput., **36**, pp. 129–134.

[21] Frisen, M., Magi, M., Sonnerup, I., and Viidik, A., 1969, "Rheological Analysis of Soft Collagenous Tissue. Part 1: Theoretical Considerations," J. Biomech., **2**, pp. 13–20.

[22] Driesen, N. J., Boerboom, R. A., Huyghe, J. M., Bouten, C. V., and Baaijens, F. P., 2003, "Computational Analyses of Mechanically Induced Collagen Fiber Remodeling in the Aortic Heart Valve," J. Biomech. Eng., **125**, pp. 549–557.

[23] Barocas, V. H., and Tranquillo, R. T., 1997, "An Anisotropic Biphasic Theory of Tissue-Equivalent Mechanics: The Interplay Among Cell Traction, Fibrillar Network Deformation, Fibril Alignment, and Cell Contact Guidance," J. Biomech. Eng., **119**, pp. 137–145.

[24] Soulhart, J., Buschmann, M. D., and Shirazi-Adl, A., 1999, "A Fibril-Network-Reinforced Biphasic Model of Cartilage in Unconfined Compression," J. Biomech. Eng., **121**, pp. 340–347.

[25] Schwartz, M. H., Leo, P. H., and Lewis, J. L., 1994, "A Microstructural Model for the Elastic Response of Articular Cartilage," J. Biomech., **27**, pp. 865–873.

[26] Jain, M. K., Chernomorsky, A., Silver, F. H., and Berg, R. A., 1988, "Material Properties of Living Soft-Tissue Composites," J. Biomed. Mater. Res., **22**, pp. 311–326.

[27] Farquhar, T., Dawson, P. R., and Torzilli, P. A., 1990, "A Microstructural Model for the Anisotropic Drained Stiffness of Articular Cartilage," J. Biomech. Eng., **112**, pp. 414–425.

[28] Lanir, Y., 1982, "Constitutive Equations for Fibrous Connective Tissues," J. Biomech., **18**, pp. 1–12.

[29] Billiar, K. L., and Sacks, M. S., 1997, "A Method to Quantify the Fiber Kinematics of Planar Tissues Under Biaxial Stretch," J. Biomech., **30**, pp. 753–756.

[30] Sawhney, R. K., and Howard, J., 2002, "Slow Local Movements of Collagen Fibers by Fibroblasts Drive the Rapid Global Self-Organization of Collagen Gels," J. Cell Biol., **157**, pp. 1083–1091.

[31] Chandran, P. L., and Barocas, V. H., 2004, "Microstructural Mechanics of Collagen Gels in Confined Compression: Poroelasticity, Viscoelasticity, and Collapse," J. Biomech. Eng., **126**, pp. 152–166.

[32] Harkness, M. L. R., 1959, "Effects of Enzymes on Mechanical Properties of Tissues," Nature (London), **183**, pp. 1821–1822.

[33] Eyre, D. R., and Wu, J. J., 1995, "Collagen Structure and Cartilage Matrix Integrity," J. Rheumatol., Suppl., **43**, pp. 82–85.

[34] Riesle, J., Hollander, A. P., Langer, R., Freed, L. E., and Vunjak-Novakovic, G., 1998, "Collagen in Tissue-Engineered Cartilage: Types, Structure, and Crosslinks," J. Cell. Biochem., **71**, pp. 313–327.

[35] Brewer, K. K., Sakai, H., Alencar, A. M., Majumdar, A., Arold, S. P., Lutchen, K. R., Ingenito, E. P., and Suki, B., 2003, "Lung and Alveolar Wall Elastic and Hysteretic Behavior in Rats: Effects of *In Vivo* Elastase Treatment," J. Appl. Physiol., **95**, pp. 1926–1936.

[36] Head, D. A., Levine, A. J., and MacKintosh, F. C., 2003, "Deformation of Cross-Linked Semiflexible Polymer Networks," Phys. Rev. Lett., **91**, p. 108102.

[37] Head, D. A., Levine, A. J., and MacKintosh, F. C., 2003, "Distinct Regimes of Elastic Response and Deformation Modes of Cross-Linked Cytoskeletal and Semiflexible Polymer Networks," Phys. Rev. E, **68**, p. 061907.

[38] Silver, F. H., Kato, Y. P., Ohno, M., and Wasserman, A. J., 1992, "Analysis of Mammalian Connective Tissue: Relationship Between Hierarchical Structures and Mechanical Properties," J. Long-Term Effects Med. Implants, **2**, pp. 165–198.

[39] Misof, K., Rapp, G., and Fratzl, P., 1997, "A New Molecular Model for Collagen Elasticity Based on Synchrotron X-Ray Scattering Evidence," Biophys. J., **72**, pp. 1376–1381.

[40] Fratzl, P., Misof, K., Zizak, I., Rapp, G., Amenitsch, H., and Bernstorff, S., 1998, "Fibrillar Structure and Mechanical Properties of Collagen," J. Struct. Biol., **122**, pp. 119–122.

[41] Mosler, E., Folkhard, W., Knorzer, E., Nemetschek-Gansler, H., Nemetschek, T., and Koch, M. H., 1985, "Stress-Induced Molecular Rearrangement in Tendon Collagen," J. Mol. Biol., **182**, pp. 589–596.

[42] Billiar, K. L., and Sacks, M. S., 2000, "Biaxial Mechanical Properties of the Native and Glutaraldehyde-Treated Aortic Valve Cusp: Part II–A Structural Constitutive Model," ASME J. Biomech. Eng., **122**, pp. 327–335.

[43] Gentleman, E., Lay, A. N., Dickerson, D. A., Nauman, E. A., Livesay, G. A., and Dee, K. C., 2003, "Mechanical Characterization of Collagen Fibers and Scaffolds for Tissue Engineering," Biomaterials, **24**, pp. 3805–3813.

[44] Sun, W., Sacks, M. S., Sellaro, T. L., Slaughter, W. S., and Scott, M. J., 2003, "Biaxial Mechanical Response of Bioprosthetic Heart Valve Biomaterials to High In-Plane Shear," J. Biomech. Eng., **125**, pp. 372–380.

[45] Kang, T., Humphrey, J. D., and Yin, F. C., 1996, "Comparison of Biaxial Mechanical Properties of Excised Endocardium and Epicardium," Am. J. Physiol., **270**, pp. H2169–H2176.

[46] Malvern, L. E., 1969, *Introduction to the Mechanics of a Continuous Medium*, Prentice–Hall, Englewood Cliffs, NJ.

[47] Lanir, Y., 1979, "A Structural Theory for the Homogeneous Biaxial Stress-Strain Relationships in Flat Collagenous Tissues," J. Biomech., **12**, pp. 423–436.

[48] Oda, M., and Iwashita, K., 1999, *Mechanics of Granular Materials: An Introduction*, Balkema, Rotterdam.

[49] Hollister, S. J., Brennan, J. M., and Kikuchi, N., 1994, "A Homogenization Sampling Procedure for Calculating Trabecular Bone Effective Stiffness and Tissue Level Stress," J. Biomech., **27**, pp. 433–444.

[50] Hollister, S. J., Fyrhie, D. P., Jepsen, K. J., and Goldstein, S. A., 1991, "Application of Homogenization Theory to the Study of Trabecular Bone Mechanics," J. Biomech., **24**, pp. 825–839.

[51] Breuls, R. G., Sengers, B. G., Oomens, C. W., Bouten, C. V., and Baaijans, F. P., 2002, "Predicting Local Cell Deformations in Engineered Tissue Constructs: A Multilevel Finite Element Approach," J. Biomech. Eng., **124**, pp. 198–207.

[52] Oda, M., Nemat-Nasser, S., and Mehrabadi, M. M., 1982, "A Statistical Study

Of Fabric in a Random Assembly of Spherical Granules," Int. J. Numer. Analyt. Meth. Geomech., **6**, pp. 77–82.
[53] Chandran, P. L., and Barocas, V. H., "Deterministic Material-Based Averaging Theory Model of Collagen Gel Micromechanics," ASME J. Biomech. Eng. (accepted).
[54] Chandran, P. L., 2005, "Microstructural Mechanics of Collagen Gels and Tissue Equivalents," Ph.D. thesis, University of Minnesota.
[55] Hoel, P. G., 1971, *Introduction to Mathematical Statistics*, Wiley, New York.
[56] Nemat-Nasser, S., and Mehrabadi, M. M., 1983, *Stress and Fabric in Granular Masses*, Elsevier, Amsterdam.
[57] Fuller, G. G., 1995, *Optical Rheometry of Complex Fluids*, Oxford University Press, New York.
[58] Bryant-Greenwood, G. D., 1998, "The Extracellular Matrix of the Human Fetal Membranes: Structure and Function," Placenta, **19**, pp. 1–11.
[59] Blondel, B., Roijen, I., and Cheneval, J. P., 1971, "Heart Cells in Culture—Simple Method for Increasing Proportion of Myoblasts," Experientia, **27**, p. 356.
[60] Hori, M., and Nemat-Nasser, S., 1999, "On Two Micromechanics Theories for Determining Micro–Macro Relations in Heterogeneous Solids," Mech. Mater., **31**, pp. 667–682.
[61] Nemat-Nasser, S., 1999, *Micromechanics: Overall Properties of Heterogeneous*, Elsevier, Amsterdam.